Ⓔ

# ATOMIC DATA AND EMISSION-LINE INTENSITIES FOR Ca VII

E. Landi[1]

Artep, Inc., Columbia, MD 21044; and US Naval Research Laboratory, Code 7660, 4555 Overlook Avenue SW, Washington, DC 20375

AND

A. K. Bhatia

NASA Goddard Space Flight Center, Greenbelt, MD 20771

## ABSTRACT

In the present work we calculate energy levels, transition probabilities, and electron-ion collisional excitation rates for the $3s^2 3p^2$, $3s 3p^3$, and $3s^2 3p 3d$ configurations of the silicon-like ion Ca VII. The total number of intermediate coupling levels considered is 27. Collision strengths are calculated at seven incident electron energies: 8, 10, 15, 20, 30, 40, and 60 ryd, using the distorted-wave approximation and a five-configuration model. Excitation rate coefficients are calculated by assuming a Maxwellian distribution of velocities and are used to calculate level populations and line emissivities under the assumption of statistical equilibrium. Line intensity ratios are calculated and compared with observed values measured from SERTS and *SOHO* CDS spectra. The diagnostic potential of Ca VII is demonstrated, with particular emphasis on the possibility of measuring the Ne/Ca relative abundance through simultaneous observations of Ca VII and Ne VI lines. Ca VII proves to be an excellent tool for the study of the first ionization potential effect in the solar transition region.

*Subject headings:* atomic data — plasmas — Sun: transition region

*On-line material:* machine-readable table

## 1. INTRODUCTION

The cosmic abundance of calcium is $2.0 \times 10^{-6}$ the abundance of hydrogen (Allen 1973, p. 31), so that lines emitted by neutral and ionized calcium are visible in astrophysical spectra. In particular, lines of Silicon-like Ca VII (Ca$^{6+}$) have been observed in the past in astrophysical and laboratory spectra by several authors. The first identifications of Ca VII lines were made in the laboratory spectra measured by Ekefors (1931), from which Whitford (1934) compiled the first list of identified Ca VII lines, later complemented by new identifications from Phillips (1939). Identified lines were observed in the EUV range between 202 and 640 Å. Subsequent laboratory spectra have helped to expand the energy level list and to improve the accuracy of the measured energies (Ekberg & Svensson 1970; Smitt, Svensson, & Outred 1976). Observations of optical lines from forbidden transitions within the ground configurations have been made in several stars: AX Persei and CI Cygni (Swings & Struve 1940), RX Puppis (Swings & Struve 1941), and RR Tel (Thackeray 1974). More recently, identifications of Ca VII lines in the EUV spectra of the Sun have been made by a few authors using data from rocket-borne and satellite-borne high-resolution spectrometers. Solar active region spectra observed by the 1989 configuration of the Solar EUV Rocket Telescope and Spectrograph (SERTS) included a few allowed Ca VII transitions in the 330–420 Å wavelength range (Thomas & Neupert 1994), while the quiet-Sun spectral atlas developed by Brooks et al. (1999) for the Coronal Diagnostic Spectrometer (CDS) on board the *Solar and Heliospheric Observatory* (*SOHO*) also reports a few Ca VII lines in that range.

Only a few authors have provided atomic data and transition rates necessary to evaluate theoretical emissivities for

Ca VII lines, and these data are either limited or incomplete. Earlier calculations of atomic parameters or transition probabilities include those by Varsavsky (1961), Malville & Berger (1965), and Krueger & Czyzak (1966). More recent systematic calculations of transition rates for Silicon-like ions (including Ca VII) were done by Huang (1985) and Fawcett (1987); the latter included only allowed transitions between the ground and the first two excited configurations. The only data set for electron-ion impact excitation available in the literature, to our knowledge, is the close-coupling calculation carried out by Galavis, Mendoza, & Zeippen (1995), which was limited to transition rates within the levels of the ground configuration only.

However, Ca VII lines can be very useful tools for the measurement of plasma parameters such as electron density and temperature, and elemental abundance. The lack of a comprehensive data set of atomic data and transition rates prevented the use of these lines for plasma diagnostics. The aim of the present work is to provide such a data set making use of the state-of-the-art computer codes from the University College, London, and a comprehensive atomic model. The distorted-wave approximation for the scattering problem is used.

Section 2 describes the approximation and the computer codes used in the present work, illustrates the atomic data and transition rates obtained, discusses their reliability, and compares them with earlier results. Section 3 reports the comparison of Ca VII line emissivities calculated with the present data set and observed line intensities from solar spectra; this section also demonstrates the diagnostic potential of Ca VII lines. Results are summarized in § 4.

## 2. THEORETICAL CALCULATIONS

The present calculation has been carried out for the three lowest configurations of Ca VII: $3s^2 3p^2$, $3s 3p^3$, and $3s^2 3p 3d$.

---

[1] Current address: Naval Research Laboratory, Code 7660, 4555 Overlook Avenue SW, Washington, DC 20375.

Energy levels have been calculated for a total of 27 fine-structure energy levels; spontaneous radiative decay rates (transition rates $A$, in $s^{-1}$) and collision strengths have been calculated for all possible transitions among these 27 levels.

The computer codes used in the present work to calculate atomic data, transition probabilities, and electron-ion impact excitation rates belong to the suite of codes developed at the University College, London.

## 2.1. *Wavefunctions and Radiative Data*

To calculate Ca VII wavefunctions and transition rates we have used the SUPERSTRUCTURE code developed by Eissner, Jones, & Nussbaumer (1974) and subsequently improved over the years. The wavefunction calculation is carried out adopting configuration-interaction type functions, which are expanded in terms of Slater-type orbitals.

The radial functions are calculated by using a modified Thomas-Fermi-Amaldi potential, which is dependent on parameters $\lambda_{nl}$ that are variationally optimized to yield the minimum term energies. The $nl$ orbitals for which the optimization was carried out are $1s$, $2s$, $2p$, $3s$, $3p$, $3d$, $4s$, $4p$, $4d$, and $4f$, and the resulting $\lambda_{nl}$ values are reported in Table 1. Several (25) configurations were used to calculate the energies and radiative decay rates for levels in the three configurations of interest: $3s^23p^2$, $3s^23p3d$, $3s^23d^2$, $3s3p^3$, $3s3p^23d$, $3s3p3d^2$, $3s3d^3, 3d^4$; $3p^33d$; $3s^23p4l$ with $l = s, p, d, f$; $3s3p^24l$ with $l = s, p, d, f$; $3p^34l$ with $l = s, p, d, f$; and $3s^23d4l$ with $l = s, p, d, f$. Relativistic corrections are included by using a Breit-Pauli Hamiltonian as a perturbation to the nonrelativistic Hamiltonian.

Energy levels are listed in Table 2, together with the observed values found in the literature. Differences between observed and theoretical energy levels are around a few percent only. We note the presence of a metastable term ($3s^23p3d\,^3F$), for which only forbidden or intercombination transitions toward lower levels are possible. In particular, while the $^3F_{2,3}$ levels can decay to the ground $^3P_{1,2}$ and $^1D_2$ levels via transitions with a relatively high $A$ value, the $^3F_4$ level can only decay through slow transitions. For this reason, the $3s^23p3d\,^3F_4$ level is significantly populated at densities greater than $5 \times 10^9$ $cm^{-3}$, typical of the solar corona, and must be taken into account for a correct evaluation of the Ca VII level populations and line emissivities. Transition rates and oscillator strengths have been calculated from the resulting wavefunctions and corrected for the differences between observed and theoretical energies whenever the latter were available for both the upper and lower levels of each transition. Forbidden transitions within the ground configurations are listed in Table 3; in this table radiative decay rates for the $3s^23p3d\,^3F$ metastable levels are also reported. The radiative transition rate of the

### TABLE 1
THOMAS-FERMI-AMALDI POTENTIAL PARAMETERS $\lambda_{nl}$ USED FOR THE WAVEFUNCTIONS CALCULATION

| Orbital | $\lambda_{nl}$ | Orbital | $\lambda_{nl}$ |
|---|---|---|---|
| $1s$ .............. | 1.42954 | $3d$.............. | 1.13289 |
| $2s$ .............. | 1.10443 | $4s$ .............. | 1.14139 |
| $2p$.............. | 1.05072 | $4p$.............. | 1.10879 |
| $3s$ .............. | 1.13815 | $4d$.............. | 1.12900 |
| $3p$.............. | 1.12004 | $4f$ .............. | 1.34717 |

### TABLE 2
THEORETICAL AND EXPERIMENTAL ENERGIES FOR Ca VII

| No. | Configuration | Level | $E_{obs}$ | $E_{th}$ |
|---|---|---|---|---|
| 1.......... | $3s^23p^2$ | $^3P_0$ | 0.0 | 0.000 |
| 2.......... | $3s^23p^2$ | $^3P_1$ | 1624.9 | 1700.388 |
| 3.......... | $3s^23p^2$ | $^3P_2$ | 4071.4 | 4265.926 |
| 4.......... | $3s^23p^2$ | $^1D_2$ | 21864.0 | 24389.123 |
| 5.......... | $3s^23p^2$ | $^1S_0$ | 48981.4 | 50811.305 |
| 6.......... | $3s3p^3$ | $^5S_2$ | 0.0 | 109858.305 |
| 7.......... | $3s3p^3$ | $^3D_1$ | 160157.5 | 159055.641 |
| 8.......... | $3s3p^3$ | $^3D_2$ | 160220.3 | 159127.703 |
| 9.......... | $3s3p^3$ | $^3D_3$ | 160529.2 | 159485.031 |
| 10......... | $3s3p^3$ | $^3P_0$ | 185256.6 | 185488.125 |
| 11......... | $3s3p^3$ | $^3P_1$ | 185392.9 | 185531.953 |
| 12......... | $3s3p^3$ | $^3P_2$ | 185412.2 | 185530.703 |
| 13......... | $3s3p^3$ | $^1D_2$ | 203616.1 | 204918.625 |
| 14......... | $3s^23p3d$ | $^3F_2$ | 0.0 | 251294.672 |
| 15......... | $3s^23p3d$ | $^3F_3$ | 0.0 | 252821.609 |
| 16......... | $3s^23p3d$ | $^3F_4$ | 0.0 | 254954.609 |
| 17......... | $3s3p^3$ | $^1P_1$ | 252489.9 | 259583.844 |
| 18......... | $3s3p^3$ | $^3S_1$ | 245240.5 | 250704.281 |
| 19......... | $3s^23p3d$ | $^3P_0$ | 289004.0 | 294410.125 |
| 20......... | $3s^23p3d$ | $^3P_1$ | 288160.0 | 293670.312 |
| 21......... | $3s^23p3d$ | $^3P_2$ | 286224.0 | 292080.062 |
| 22......... | $3s^23p3d$ | $^1D_2$ | 0.0 | 296811.625 |
| 23......... | $3s^23p3d$ | $^3D_1$ | 295138.0 | 301837.781 |
| 24......... | $3s^23p3d$ | $^3D_2$ | 295772.0 | 302536.375 |
| 25......... | $3s^23p3d$ | $^3D_3$ | 296132.0 | 303000.531 |
| 26......... | $3s^23p3d$ | $^1F_3$ | 324885.0 | 334259.031 |
| 27......... | $3s^23p3d$ | $^1P_1$ | 333501.0 | 341655.000 |

NOTE.—Experimental energies come from the NIST database (Fuhr et al. 1999), with the only exception of level 18 ($3s3p^3\,^1P_1$), which is taken from Kelly 1987.

$3s3p^3\,^3D_3$–$3s^23p3d\,^3F_4$ transition contains a nonnegligible contribution from a magnetic dipole transition, which has been added to the $A$ value reported in Table 3.

Table 4 lists the transition rates for optically allowed transitions between the ground configuration and the $3s3p^3$ configuration, while Table 5 gives the optically allowed transitions between levels in the ground configuration and in the $3s^23p3d$ excited configuration.

## 2.2. *Collision Strengths*

The electron-ion scattering problem is carried out in the distorted-wave (DW) approximation (Eissner & Seaton 1972). The programs used in the present work are described in Eissner (1998) and have been improved throughout the years.

The atomic model used for the scattering problem is simpler than the one adopted in the wavefunction calculation, because of computer memory constraints. The configuration included in the calculation are five: $3s^23p^2$, $3s^23p3d$, $3s3p^3$, $3p^4$, and $3s^23d^2$. In the present work we report the collision strengths for only the first three of these configurations. The reactance matrices are calculated in $LS$ coupling. The results are converted into intermediate coupling by using the term coupling coefficients calculated in SUPERSTRUCTURE for this 5 configuration model, and the program developed by Saraph (1978).

The calculations have been carried out explicitly by using intermediate angular momentum states $L^T$ up to 32, with $L^T = l_i + l_t$, where $l_i$ is the angular momentum of the

FORBIDDEN RADIATIVE TRANSITION PROBABILITIES FOR TRANSITIONS BETWEEN LEVELS WITHIN THE
GROUND CONFIGURATION, AND FOR TRANSITIONS INVOLVING THE METASTABLE $3s^23p3d$ $^3F$ TERM

| DOWN | UP | TRANSITION | WAVELENGTH (Å) | TYPE | $A$ (s$^{-1}$) 5 Configuration | $A$ (s$^{-1}$) 25 Configuration |
|---|---|---|---|---|---|---|
| | | | $3s^23p^2$–$3s^23p^2$ | | | |
| 1 | 2 | $^3P_0$–$^3P_1$ | 61542.362 | M1 | 7.668E−02 | 7.638E−02 |
| 1 | 3 | $^3P_0$–$^3P_2$ | 24561.621 | E2 | 1.620E−05 | 1.979E−05 |
| 1 | 4 | $^3P_0$–$^1D_2$ | 4573.737 | E2 | 2.717E−04 | 1.072E−03 |
| 2 | 3 | $^3P_1$–$^3P_2$ | 40874.794 | M1 | 1.955E−01 | 1.958E−01 |
| 2 | 4 | $^3P_1$–$^1D_2$ | 4940.940 | M1 | 1.076E+00 | 9.256E−01 |
| 2 | 5 | $^3P_1$–$^1S_0$ | 2111.647 | M1 | 3.474E+01 | 5.685E+01 |
| 3 | 4 | $^3P_2$–$^1D_2$ | 5620.324 | M1 | 2.173E+00 | 1.872E+00 |
| 3 | 5 | $^3P_2$–$^1S_0$ | 2226.680 | E2 | 1.876E−01 | 1.115E−01 |
| 4 | 5 | $^1D_2$–$^1S_0$ | 3687.676 | E2 | 4.379E+00 | 5.186E+00 |
| | | | Transitions involving the $3s^23p3d$ $^3F_4$ level | | | |
| 3 | 16 | $3s^23p^2$ $^3P_2$–$^3F_4$ | 398.902[a] | M2 | 2.623E+00 | 2.867E+00 |
| 4 | 16 | $3s^23p^2$ $^1D_2$–$^3F_4$ | 433.717[a] | M2 | 5.147E+00 | 5.318E+00 |
| 6 | 16 | $3s3p^3$ $^5S_2$–$^3F_4$ | 689.199[a] | E2 | 4.051E−01 | 1.732E−01 |
| 8 | 16 | $3s3p^3$ $^3D_2$–$^3F_4$ | 1043.550[a] | E2 | 1.119E+00 | 1.396E+00 |
| 9 | 16 | $3s3p^3$ $^3D_3$–$^3F_4$ | 1047.456[a] | E2[b] | 1.056E+00 | 2.183E+00 |
| 12 | 16 | $3s3p^3$ $^3P_2$–$^3F_4$ | 1440.429[a] | E2 | 1.293E+01 | 1.177E+01 |
| 13 | 16 | $3s3p^3$ $^1D_2$–$^3F_4$ | 1998.565[a] | E2 | 1.829E−02 | 5.480E−03 |
| 14 | 16 | $3s^23p3d$ $^3F_2$–$^3F_4$ | 27322.922[a] | E2 | 5.775E−07 | 5.905E−07 |
| 15 | 16 | $3s^23p3d$ $^3F_3$–$^3F_4$ | 46882.410[a] | M1 | 1.961E−01 | 1.693E−01 |
| | | | Transitions involving the $3s^23p3d$ $^3F_{2,3}$ levels | | | |
| 2 | 14 | $3s^23p^2$ $^3P_1$–$^3F_2$ | 400.651[a] | E1 | 7.806E+06 | 7.075E+06 |
| 3 | 14 | $3s^23p^2$ $^3P_2$–$^3F_2$ | 404.812[a] | E1 | 4.102E+06 | 3.378E+06 |
| 4 | 14 | $3s^23p^2$ $^1D_2$–$^3F_2$ | 440.713[a] | E1 | 1.961E+07 | 1.512E+07 |
| 3 | 15 | $3s^23p^2$ $^3P_2$–$^3F_3$ | 402.325[a] | E1 | 1.733E+07 | 1.536E+07 |
| 4 | 15 | $3s^23p^2$ $^1D_2$–$^3F_3$ | 437.767[a] | E1 | 4.495E+06 | 4.475E+06 |

NOTE.—Results from the 5 configuration model are also reported for comparison purposes. Wavelengths
are calculated using experimental energy levels.

[a] Wavelengths calculated using the theoretical levels.

[b] The radiative transition rate of the $3s3p^3$ $^3D_3$–$3s^23p3d$ $^3F_4$ transition contains a nonnegligible contribution
from a magnetic dipole transition, which has been added to the $A$ value reported in the table.

SPONTANEOUS RADIATIVE DECAY RATES FOR OPTICALLY ALLOWED
TRANSITIONS $3s^23p^2$—$3s3p^3$

| DOWN | UP | TRANSITION | WAVELENGTH (Å) | $A$ (s$^{-1}$) 25 Configuration | $A$ (s$^{-1}$) 5 Configuration |
|---|---|---|---|---|---|
| 1 | 7 | $^3P_0$–$^3D_1$ | 624.387 | 3.092E+08 | 3.038E+08 |
| 1 | 11 | $^3P_0$–$^3P_1$ | 539.396 | 4.926E+08 | 8.269E+08 |
| 1 | 18 | $^3P_0$–$^3S_1$ | 407.764 | 3.486E+09 | 3.593E+09 |
| 2 | 7 | $^3P_1$–$^3D_1$ | 630.786 | 1.615E+08 | 1.491E+08 |
| 2 | 8 | $^3P_1$–$^3D_2$ | 630.537 | 4.024E+08 | 3.991E+08 |
| 2 | 10 | $^3P_1$–$^3P_0$ | 544.569 | 1.508E+09 | 2.518E+09 |
| 2 | 11 | $^3P_1$–$^3P_1$ | 544.165 | 4.792E+08 | 7.406E+08 |
| 2 | 12 | $^3P_1$–$^3P_2$ | 544.108 | 2.928E+08 | 5.327E+08 |
| 2 | 18 | $^3P_1$–$^3S_1$ | 410.484 | 9.917E+09 | 1.077E+10 |
| 3 | 8 | $^3P_2$–$^3D_2$ | 640.416 | 6.468E+07 | 5.396E+07 |
| 3 | 9 | $^3P_2$–$^3D_3$ | 639.151 | 4.450E+08 | 4.292E+08 |
| 3 | 11 | $^3P_2$–$^3P_1$ | 551.508 | 5.131E+08 | 9.092E+08 |
| 3 | 12 | $^3P_2$–$^3P_2$ | 551.449 | 1.133E+09 | 1.864E+09 |
| 3 | 18 | $^3P_2$–$^3S_1$ | 414.648 | 1.670E+10 | 1.583E+10 |
| 4 | 13 | $^1D_2$–$^1D_2$ | 550.201 | 1.825E+09 | 1.838E+09 |
| 4 | 17 | $^1D_2$–$^1P_1$ | 433.603 | 1.470E+10 | 1.443E+10 |
| 5 | 17 | $^1S_0$–$^1P_1$ | 491.381 | 1.602E+09 | 6.632E+08 |

NOTE.—Wavelengths are calculated using the experimental energies. Results from the 5
configuration model are also reported for comparison purposes.

LANDI & BHATIA

TABLE 5
SPONTANEOUS RADIATIVE DECAY RATES FOR OPTICALLY ALLOWED
TRANSITIONS $3s^2 3p^2$—$3s^2 3p 3d$

| | | | WAVELENGTH | $A$ (s$^{-1}$) | |
| DOWN | UP | TRANSITION | (Å) | 25 Configuration | 5 Configuration |
|---|---|---|---|---|---|
| 1 | 20 | $^3P_0$–$^3P_1$ | 347.030 | 1.258E+10 | 1.377E+10 |
| 1 | 23 | $^3P_0$–$^3D_1$ | 338.825 | 1.741E+10 | 2.180E+10 |
| 2 | 19 | $^3P_1$–$^3P_0$ | 347.973 | 2.520E+10 | 2.863E+10 |
| 2 | 20 | $^3P_1$–$^3P_1$ | 348.998 | 3.304E+09 | 3.938E+09 |
| 2 | 23 | $^3P_1$–$^3D_1$ | 340.701 | 1.918E+10 | 2.277E+10 |
| 2 | 24 | $^3P_1$–$^3D_2$ | 339.967 | 2.429E+10 | 3.027E+10 |
| 3 | 20 | $^3P_2$–$^3P_1$ | 352.004 | 9.271E+09 | 1.076E+10 |
| 3 | 21 | $^3P_2$–$^3P_2$ | 354.419 | 1.348E+10 | 1.607E+10 |
| 3 | 23 | $^3P_2$–$^3D_1$ | 343.565 | 2.331E+09 | 2.602E+09 |
| 3 | 24 | $^3P_2$–$^3D_2$ | 342.818 | 1.422E+10 | 1.649E+10 |
| 3 | 25 | $^3P_2$–$^3D_3$ | 342.395 | 3.823E+10 | 4.626E+10 |
| 4 | 22 | $^1D_2$–$^1D_2$ | 367.078[a] | 3.170E+10 | 4.427E+10 |
| 4 | 26 | $^1D_2$–$^1F_3$ | 330.011 | 4.193E+10 | 5.133E+10 |
| 4 | 27 | $^1D_2$–$^1P_1$ | 320.887 | 3.909E+07 | 5.262E+09 |
| 5 | 27 | $^1S_0$–$^1P_1$ | 351.470 | 3.198E+10 | 3.127E+10 |

NOTE.—Wavelengths are calculated using the experimental energies, where available, otherwise with the theoretical values. Results from the 5 configuration model are also reported for comparison purposes.

[a] Calculated with theoretical values.

incident electron and $l_t$ is the angular momentum of the target level. The nonnegligible contribution from higher partial waves has been taken into account both for optically allowed and for forbidden transitions. Higher partial wave contributions for optically allowed transitions have been accounted for by using the Coulomb-Bethe approximation, according to Burgess & Shoerey (1974); contributions to forbidden transitions have been estimated by using a geometrical progression. These contributions have been included in the intermediate coupling program of Saraph & Eissner (2003). The calculations have been carried out for seven values of the incident electron energy: 8, 10, 15, 20, 30, 40, and 60 ryd.

Care has been taken to ensure the convergence of all collision strengths with respect to $L^T$. Table 6 reports the collision strengths of a few sample transitions obtained at increasing values of $L^T$. It can be seen that the collision strengths have already converged at $L^T = 21$.

Resulting collision strengths for all possible transitions within the adopted Ca VII atomic model are reported in Table 7. These collision strengths have also been scaled and fitted according to Burgess & Tully (1992), and integrated over a Maxwellian distribution of velocities to yield excitation rate coefficients. Results are stored in the format of the CHIANTI database (Dere et al. 1997; Young et al. 2003), and will be released in the next version of the database.

TABLE 6
COLLISION STRENGTHS AS A FUNCTION OF THE MAXIMUM VALUE OF THE ANGULAR MOMENTUM $L^T$

| | $L^T$ | | | | |
| TRANSITION | 11 | 16 | 21 | 26 | 32 |
|---|---|---|---|---|---|
| 1–7......................... | 7.515E−01 | 7.183E−01 | 7.171E−01 | 7.167E−01 | 7.164E−01 |
| 2–8......................... | 1.757E+00 | 1.632E+00 | 1.628E+00 | 1.628E+00 | 1.627E+00 |
| 2–4......................... | 4.099E−03 | 6.648E−03 | 6.6778E−03 | 6.810E−03 | 6.844E−03 |
| 2–5......................... | 1.750E−04 | 1.550E−04 | 1.550E−04 | 1.550E−04 | 1.550E−04 |
| 7–8......................... | 1.401E−02 | 9.744E−03 | 9.827E−03 | 9.836E−03 | 9.836E−03 |
| 3–18....................... | 1.103E+01 | 9.827E+00 | 9.699E+00 | 9.680E+00 | 9.673E+00 |
| 3–20....................... | 4.234E+00 | 3.709E+00 | 3.648E+00 | 3.641E+00 | 3.639E+00 |
| 2–22....................... | 6.187E−02 | 5.429E−02 | 5.338E−02 | 5.321E−02 | 5.306E−02 |
| 19–26..................... | 6.320E−04 | 5.180E−04 | 5.150E−04 | 5.150E−04 | 5.150E−04 |
| 11–27..................... | 7.230E−04 | 5.130E−04 | 5.220E−04 | 5.220E−04 | 5.230E−04 |
| 22–27..................... | 1.374E+00 | 1.145E+00 | 1.010E+00 | 1.012E+00 | 1.022E+00 |
| 17–27..................... | 2.252E−02 | 5.517E−02 | 5.081E−02 | 5.093E−02 | 5.133E−02 |
| 20–25..................... | 6.037E−01 | 4.954E−01 | 4.411E−01 | 4.411E−01 | 4.448E−01 |
| 14–25..................... | 6.830E−03 | 1.440E−02 | 1.327E−02 | 1.319E−02 | 1.322E−02 |

NOTE.—Calculations were carried out at the highest incident electron energy used in the present work: 60 ryd. The collision strengths are nearly constant for $L^T > 21$, thus showing that they have converged. Convergence at lower incident electron energies occurs for even smaller values of $L^T$.

TABLE 7
Oscillator Strengths and Collision Strengths for Ca VII

| Down | Up | Oscillator Strength | $\Omega$ (8 ryd) | $\Omega$ (10 ryd) | $\Omega$ (15 ryd) | $\Omega$ (20 ryd) | $\Omega$ (30 ryd) | $\Omega$ (40 ryd) | $\Omega$ (60 ryd) |
|---|---|---|---|---|---|---|---|---|---|
| 1 | 2 | | 4.919E−02 | 3.908E−02 | 2.461E−02 | 1.715E−02 | 9.755E−03 | 6.287E−03 | 3.215E−03 |
| 1 | 3 | | 2.152E−01 | 2.162E−01 | 2.192E−01 | 2.230E−01 | 2.278E−01 | 2.320E−01 | 2.339E−01 |
| 1 | 4 | | 2.030E−02 | 1.654E−02 | 1.112E−02 | 8.359E−03 | 5.702E−03 | 4.514E−03 | 3.479E−03 |
| 1 | 5 | | 1.543E−03 | 1.138E−03 | 6.210E−04 | 3.930E−04 | 2.000E−04 | 1.180E−04 | 5.700E−05 |
| 1 | 6 | | 1.342E−02 | 1.105E−02 | 7.064E−03 | 4.824E−03 | 2.643E−03 | 1.671E−03 | 8.500E−04 |
| 1 | 7 | 5.330E−02 | 4.527E−01 | 4.761E−01 | 5.234E−01 | 5.599E−01 | 6.153E−01 | 6.564E−01 | 7.164E−01 |
| 1 | 8 | | 1.991E−02 | 1.631E−02 | 1.038E−02 | 7.083E−03 | 3.875E−03 | 2.447E−03 | 1.243E−03 |
| 1 | 9 | | 3.673E−03 | 3.596E−03 | 3.570E−03 | 3.607E−03 | 3.748E−03 | 3.875E−03 | 4.054E−03 |
| 1 | 10 | | 2.195E−03 | 1.801E−03 | 1.141E−03 | 7.730E−04 | 4.170E−04 | 2.600E−04 | 1.290E−04 |
| 1 | 11 | 1.083E−01 | 7.149E−01 | 7.609E−01 | 8.521E−01 | 9.208E−01 | 1.024E+00 | 1.099E+00 | 1.208E+00 |

Note.—All data have been calculated with the 5 configuration model, for self-consistency. Table 7 is published in its entirety in the electronic edition of the Astrophysical Journal. A portion is shown here for guidance regarding its form and content.

### 2.3. Reliability of the Results

The accuracy of the present collisional results is limited by two main factors: (1) the neglect of resonances and (2) the limited size of the target's model in the collisional calculation. Assessing the effect of resonances on collision strengths for Ca VII is very difficult, because of the lack of accurate R-matrix calculations; these are hindered by the lack of accurate measurements of energies of the states of interest, as pointed out by Galavis et al. (1995).

In order to investigate the effects of neglecting all the configurations in the $n = 3$ complex except the five we have considered, we have examined the contribution of all the configurations left out on the wavefunctions of the energy levels of the $3s^2 3p^2$, $3s3p^3$, and $3s^2 3p3d$ configurations. We compared the wavefunctions obtained with the 5 and 25 configuration models, and found that the only significant contributions (i.e., with percentage contribution larger than 0.5%) are given by the $3s^2 3d^2$, $3s3p^2 3d$, and $3p^4$ configurations to the levels in the ground configuration, and by the $3s3p3d^2$ and $3p^3 3d$ configurations to the $3s3p^3$ and $3s^2 3p3d$ ones. However, because of computer memory constraints, it has been possible to include only the $3s^2 3d^2$ and $3p^4$ configurations in the target model. This means that the wavefunctions of all configurations considered in the present work might have limited accuracy. However, the neglected percentage contributions from the $3s3p^2 3d$, $3s3p3d^2$, and $3p^3 3d$ levels is never larger than 2.5%, with the only exception of the $3s3p^3\,{}^3S_1$ level, whose wavefunction includes a 4.6% contribution from a $3p^3 3d\,{}^3S_1$ level.

Tables 3, 4, and 5 report the A values obtained with the 5 configuration model, for comparison with the results from the 25 configuration model adopted in the present work. It is possible to see that in most cases the A values agree within 20%, but in some cases much larger discrepancies are found. These discrepancies give an idea of the inaccuracies in the target wavefunctions that occurred with the neglect of the $3s3p3d^2$ and $3p^3 3d$ configurations, and of the levels affected by them.

Unfortunately, it is not possible to carry out a similar comparison for the collision strengths.

### 2.4. Comparison with Earlier Work

Only a few calculations of atomic data and transition rates for Ca VII are available in the literature. To our knowl-edge, radiative data have been calculated by Huang (1985) and Fawcett (1987), while collision transition probabilities have been computed by Galavis et al. (1995).

Both Huang (1985) and Fawcett (1987) calculated radiative data for the whole Si-like isoelectronic sequence. Huang (1985) used the multiconfiguration-Dirac-Fock computer code by Desclaux (1975) to calculate electric quadrupole and magnetic dipole transitions within the ground configuration and electric dipole transition rates between the ground levels and the levels of two excited configurations. This author included in his calculations all the configurations in the $n = 3$ complex. Fawcett (1987) instead provides data only for optically allowed transitions, calculated using a Hartree-Fock-relativistic computer code that took into account configuration interaction, and optimized the Slater parameters in order to minimize differences between computed and observed wavelengths. The $3s^2 3p^2$, $3s3p^3$, $3s^2 3p3d$, $3p^4$, $3s3p^2 3d$, $3p^3 3d$, $3s3p3d^2$, and $3s^2 3p^4 s$ were included in the Fawcett (1987) calculation. A comparison between the present results and those from Huang (1985) and Fawcett (1987) is reported in Table 8. It can be seen that the results from the three different computations are in good agreement with each other. The largest differences arise between the present results and the Huang data for a few forbidden lines, whose effect on the overall level populations is, however, negligible.

The only calculations of collisional excitation rates for Ca VII transitions have been carried out by Galavis et al. (1995). They used the close-coupling approximation to calculate fine-structure collision strengths for infrared transitions within the ground term. Their calculations involved silicon-like ions from S III to Ca VII. Effective collision strengths, including resonance contributions, were calculated in the temperature range $10^3$–$10^5$ K. However, a detailed comparison between this data set and the results of the present work is not possible, since the temperature range considered by Galavis et al. (1995) is much lower than the range where Ca VII is significantly abundant; our calculations provide collision strengths at energies typical of much hotter plasmas, and the extrapolation at much lower temperatures, made through the Burgess & Tully (1992) scaling laws, might introduce additional problems. Moreover, Galavis et al. (1995) point out the lack of measured energies of highly excited states giving rise to resonances in the ground transitions. This lack causes the location of the

## TABLE 8
COMPARISON OF SPONTANEOUS RADIATIVE DECAY OBTAINED IN THE
PRESENT WORK WITH VALUES AVAILABLE IN THE LITERATURE

| Transition | Present | Fawcett[a] | Huang |
|---|---|---|---|
| $3s^23p^2$–$3s^23p^2$ | | | |
| $^3P_0$–$^3P_1$ ................. | 7.668E−02 | | 8.164E−02 |
| $^3P_1$–$^3P_2$ ................. | 1.955E−01 | | 1.959E−01[b] |
| $^3P_1$–$^1D_2$ ................. | 1.446E+00 | | 1.076E+00[b] |
| $^3P_1$–$^1S_0$ ................. | 3.861E+01 | | 3.474E+01 |
| $^3P_2$–$^1D_2$ ................. | 3.350E+00 | | 2.173E+00[b] |
| $^3P_0$–$^3P_2$ ................. | 1.699E−05 | | 1.620E−05 |
| $^3P_0$–$^1D_2$ ................. | 7.872E−04 | | 2.717E−04 |
| $^3P_2$–$^1S_0$ ................. | 2.436E−01 | | 1.876E−01 |
| $^1D_2$–$^1S_0$ ................. | 5.558E+00 | | 4.379E+00 |
| $3s^23p^2$–$3s3p^3$ | | | |
| $^3P_2$–$^3S_1$ ................. | 1.669E+10 | 1.661E+10 | 1.828E+10[c] |
| $^3P_2$–$^3D_3$ ................. | 4.449E+08 | 3.832E+08 | 4.316E+08 |
| $^3P_1$–$^3P_2$ ................. | 2.927E+08 | 2.603E+08 | 2.712E+08 |
| $^3P_2$–$^3P_1$ ................. | 5.131E+08 | 4.452E+08 | 4.844E+08 |
| $^3P_0$–$^3P_1$ ................. | 4.926E+08 | 4.334E+08 | 4.696E+08 |
| $^1D_2$–$^1P_1$ ................. | 1.469E+10 | 1.521E+10 | 1.533E+10[c] |
| $^1S_0$–$^1P_1$ ................. | 1.602E+09 | 1.160E+09 | 2.148E+09[c] |
| $3s^23p^2$–$3s^23p3d$ | | | |
| $^3P_2$–$^3D_3$ ................. | 3.823E+10 | 3.899E+10 | 4.103E+10 |
| $^3P_1$–$^3P_2$ ................. | 9.791E+09 | 1.042E+10 | 1.170E+10 |
| $^3P_2$–$^3P_1$ ................. | 9.274E+09 | 9.716E+09 | 9.895E+09 |
| $^3P_0$–$^3P_1$ ................. | 1.258E+10 | 1.371E+10 | 1.257E+10 |
| $^1D_2$–$^1F_3$ ................. | 4.193E+10 | 4.277E+10 | 4.460E+10 |
| $^1S_0$–$^1P_1$ ................. | 3.198E+10 | 3.617E+10 | 3.434E+10 |
| $^3P_1$–$^3F_2$ ................. | 7.817E+06 | | 4.554E+06 |
| $^3P_2$–$^3F_2$ ................. | 4.100E+06 | | 3.111E+06 |
| $^3P_2$–$^3F_3$ ................. | 1.733E+07 | | 1.696E+07 |

[a] Fawcett transition rates have been calculated by using the *gf* values and theoretical wavelengths reported in his Table 1.

[b] The *A* value for these transitions have been obtained by summing the E1 and M2 transition probabilities given by Huang 1985.

[c] The Huang transition probabilities for levels $3s3p^3$ $^3S_1$ and $^1P_1$ have been exchanged because of exchanged labeling of the upper levels in Huang 1985.

resonances to be uncertain and compromises the accuracy of their close-coupling results. A comparison between close-coupling and DW results would be enlightening in understanding the importance of resonances in the rate coefficients for Ca VII.

## 3. COMPARISON WITH OBSERVATIONS

### 3.1. Ca VII *Line Emissivities and Their Diagnostic Potential*

In the absence of absorption of the solar blackbody radiation and proton excitations, level populations and line emissivities are obtained by solving the equations of statistical equilibrium, under steady-state conditions ($dN_i/dt = 0$):

$$- N_e N_i \left( \sum_{j>i} C_{ij}^e + \sum_{j<i} C_{ij}^d \right) + \sum_{j>i} A_{ji}$$
$$- N_i \sum_{j<i} A_{ij} + N_e \left( \sum_{j>i} N_j C_{ji}^d + \sum_{j<i} N_j C_{ji}^e \right) = 0 , \quad (1)$$

where $N_j$ is the number density of level $j$, $N_e$ is the electron density, and $A_{ji}$ (s$^{-1}$) is the spontaneous radiative transition rate from level $j$ to level $i$. Here $C_{ij}^e$ and $C_{ji}^d$ are the electron collision excitation and de-excitation rate coefficients between levels $i$ and $j$, and $C_{ij}^e$ is defined as

$$C_{i,j}^e = \frac{8.63 \times 10^{-6}}{\omega_i T_e^{1/2}} \exp\left( -\frac{E_{i,j}}{kT_e} \right)$$
$$\times \int_0^\infty \Omega_{i,j} \exp\left( -\frac{E_j}{kT_e} \right) d\left( \frac{E_j}{kT_e} \right) , \quad (2)$$

where $\omega_i$ is the statistical weight of level $i$, $E_{i,j}$ is the energy difference between levels $i$ and $j$, $k$ is the Boltzmann constant, and $E_j$ is the energy of the scattered electron relative to the final energy state of the ion.

Ca VII gives rise to several groups of transitions, a few of which have been observed in the past. The strongest lines are emitted in the EUV spectral range. Table 9 lists the strongest transitions and their wavelengths. Ca VII emission lines are density sensitive mostly in the $10^4$–$10^8$ cm$^{-3}$ density range, making them unfit for density diagnostics in the solar transition region, where the electron density is usually higher, but suitable for diagnostics of less dense astrophysical plasmas. The only lines that can potentially provide useful density-sensitive line ratios for the solar atmosphere, and that are sufficiently strong to be observed, are those involving singlet levels. These are marked by an asterisk in Table 9. These lines are density sensitive in the $10^7$–$10^9$ cm$^{-3}$ range. An example of density-sensitive Ca VII line ratios is displayed in Figure 1 (*top*).

Ca VII emits strong optically allowed lines coming from two upper configurations well separated in energy. This means that line ratios from one line emitted by a $3s^23p3d$ upper level and one line coming from a $3s3p^3$ upper level will be temperature sensitive. Also, some relative temperature sensitivity is also present within the $3s3p^3$, when ratios between one $^3P$–$^3S$ line and one of the $^3P$–$^3P$ or $^3P$–$^3D$ lines

## TABLE 9
STRONGEST MULTIPLETS AND LINES
EMITTED BY Ca VII

| Transition | Wavelength (Å) |
|---|---|
| $3s^23p^2$–$3s^23p3d$ | |
| $^3P$–$^3D$ ........................... | 338–343 |
| $^3P$–$^3P$ ........................... | 347–354 |
| $^1D_2$–$^1F_3$ ........................ | 330.01* |
| $^1S_0$–$^1P_1$ ........................ | 351.47* |
| $3s^23p^2$–$3s3p^3$ | |
| $^3P$–$^3S$ ........................... | 410–433 |
| $^3P$–$^3P$ ........................... | 539–551 |
| $^3P$–$^3D$ ........................... | 624–640 |
| $3s^23p^2$–$3s^23p^2$ | |
| $^3P_1$–$^1S_0$ ....................... | 2111.65 |
| $^3P_1$–$^1D_2$ ....................... | 4940.94 |
| $^3P_2$–$^1D_2$ ....................... | 5620.32 |
| $^3P_0$–$^3P_1$ ....................... | 61542.99 |
| $^3P_1$–$^3P_2$ ....................... | 40874.99 |

NOTE.—Lines marked with an asterisk are strongly density sensitive at densities typical of the solar transition region.
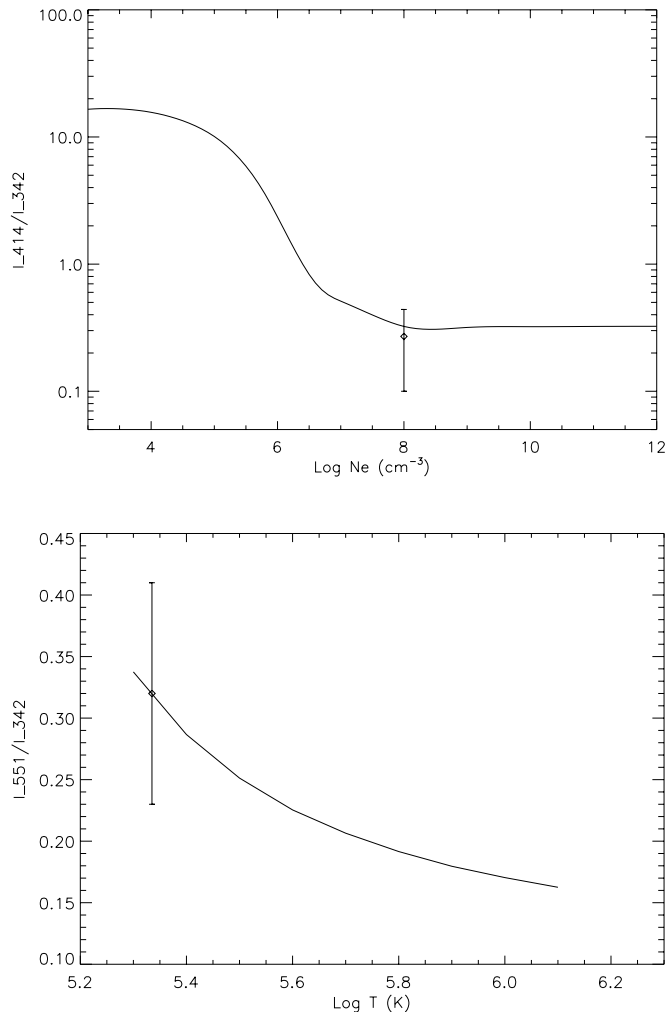
FIG. 1.—*Top*: Theoretical estimate of the 414.65/342.40 line intensity ratio as a function of the electron density, calculated assuming $\log T = 5.7$ (*T* in K). The observed value comes from SERTS active region observations (see § 3.2). *Bottom*: Theoretical estimate of the (551.45 + 551.51)/342.40 line intensity ratio as a function of the electron temperature, calculated assuming $\log N_e = 9.0$ ($N_e$ in cm$^{-3}$). The observed value comes from CDS active region observations (see § 3.3).

are considered. An example of a temperature-sensitive Ca VII line ratio is displayed in Figure 1 (*bottom*).

Ca VII lines can be used to study element abundances in the solar transition region. Ca VII abundance peaks at $\log T \simeq 5.65$ (*T* in K), very close to the Ne VI maximum abundance temperature. Moreover, several Ne VI lines are close in wavelength to Ca VII transitions: lines from the two ions are included in the wavelength range of the CDS instrument on *SOHO*, and of the 1989 configuration of the Solar EUV Rocket Telescope and Spectrograph (SERTS). Figure 2 (*top*) shows the contribution function of the Ca VII 342.40 Å line and of the Ne VI 562.80 Å doublet, and demonstrates that the temperature range of formation of these lines is nearly identical. This makes it possible to study the relative abundance of Ca and Ne.

The first ionization potential (FIP) of calcium is 6.1 eV, while the neon value is 21.6 eV. This makes Ca VII and Ne VI an excellent pair of ions for studying the FIP effect. This effect consists of systematic differences between photospheric and coronal element abundances. The latter show enhancements of a factor of around 4 in the so-called low-

FIP elements (FIP $\leq$ 10 eV), while abundances for the high-FIP elements (FIP > 10 eV) remain constant between the photosphere and the corona. So far, no theoretical model has been able to satisfactorily explain this effect.

One of the most used methods for the measurement of relative abundances between two elements consists of comparing a theoretical estimate of the ratio of two lines by assuming that their temperature dependence is identical (i.e., Young & Mason 1997). However, the ratio of the Ca VII 342.40 Å and Ne VI 561.72 Å lines, displayed in Figure 2 (*bottom*), shows that its temperature dependence is not negligible and can significantly affect any measurement of relative abundance. These two lines can be confidently used for relative abundance measurements and FIP effect studies only through a differential emission measure (DEM) study as described by Del Zanna, Landini, & Mason (2002) and references therein.

### 3.2. *SERTS Data*

Ca VII lines have been observed by SERTS on two occasions. Two lines were reported in the spectrum recorded in the 1989 flight (Thomas & Neupert 1994), while only one
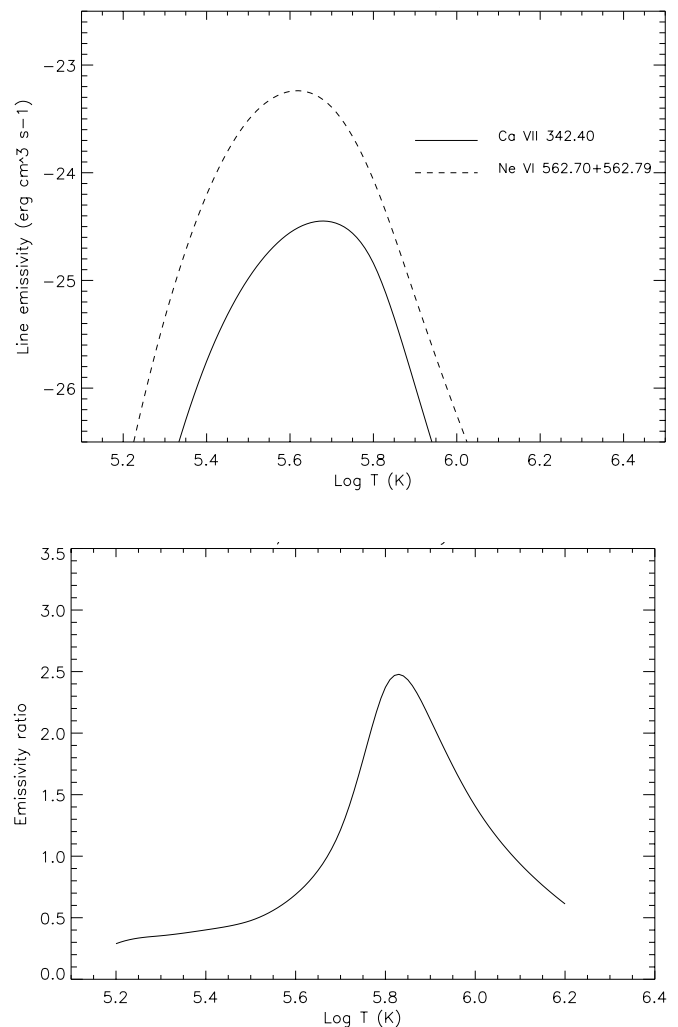


FIG. 2.—*Top*: Contribution functions of the Ca VII 342.40 Å line and of the Ne VI 562.80 Å doublet as a function of electron temperature. *Bottom*: Emissivity ratio between the Ca VII 342.40 Å line and of the Ne VII 562.80 Å doublet as a function of electron temperature. The electron density has been assumed to be $N_e = 10^9$ cm$^{-3}$.

TABLE 10
COMPARISON BETWEEN OBSERVED AND THEORETICAL LINE INTENSITIES FOR Ca VII

| Transition | $\lambda_{\mathrm{obs}}$ (Å) | $\lambda_{\mathrm{th}}$ (Å) | Intensity | Observed Ratio | Theoretical Ratio | Diagnostics |
|---|---|---|---|---|---|---|
| SERTS 1989 (Intensity in ergs cm$^{-2}$ s$^{-1}$ sr$^{-1}$) | | | | | | |
| $3s^23p^2\,^3P_2$–$3s^23p3d\,^3D_3$ ............. | 342.390 | 342.395 | $13.2 \pm 5.9$ | 1.0 | 1.0 | |
| $3s^23p^2\,^3P_2$–$3s3p^3\,^3S_1$ ................. | 414.679 | 414.648 | $3.5 \pm 1.6$ | $0.27 \pm 0.17$ | $0.37 \pm 0.02$ | $\log N_e > 7.2$ |
| CDS: Quiet Sun (Intensity in counts s$^{-1}$ pixel$^{-1}$) | | | | | | |
| $3s^23p^2\,^3P_1$–$3s^23p3d\,^3D_2$ ............. | 339.891 | 339.967 | $0.007 \pm 0.004$ | $0.64 \pm 0.38$ | $0.46 \pm 0.01$ | $\log N_e > 6.7$ |
| $3s^23p^2\,^3P_2$–$3s^23p3d\,^3D_3$ ............. | 342.454 | 342.395 | $0.011 \pm 0.002$ | 1.0 | 1.0 | |
| CDS: Active Region (Intensity in ergs cm$^{-2}$ s$^{-1}$ sr$^{-1}$) | | | | | | |
| $3s^23p^2\,^1D_2$–$3s^23p3d\,^1F_3$ ............. | 329.928 | 330.011 | $28.3 \pm 1.5$ | $1.49 \pm 0.42$ | 0.02–0.8[a] | |
| $3s^23p^2\,^3P_1$–$3s^23p3d\,^3D_2$ ............. | 339.918 | 339.967 | $11.8 \pm 2.7$ | $0.62 \pm 0.18$ | $0.46 \pm 0.01$ | $\log N_e > 7.0$ |
| $3s^23p^2\,^3P_1$–$3s^23p3d\,^3D_1$ ............. | 340.722 | 340.701 | $16.9 \pm 2.6$ | $0.89 \pm 0.25$ | $0.22 \pm 0.003$ | $\log N_e = 6.8^{+0.2}_{-0.1}$ |
| $3s^23p^2\,^3P_2$–$3s^23p3d\,^3D_3$ ............. | 342.445 | 342.395 | $19.0 \pm 2.2$ | 1.0 | 1.0 | |
| $3s^23p^2\,^3P_2$–$3s3p^3\,^3P_2$ ................. | 551.471 | 551.449 | $6.1 \pm 0.5$ | $0.32 \pm 0.09$ | $0.20 \pm 0.003$ | $\log T \leq 5.55$ |
| $3s^23p^2\,^3P_2$–$3s3p^3\,^3P_1$ ................. | | 551.508 | | | | |

NOTE.—The theoretical estimates are given as the average of the intensity ratio values calculated at $\log N_e = 8$, 9, 10, 11, and 12 assuming $\log T = 5.7$ ($T$ in K), and their uncertainties as the standard deviation.

[a] The 330.01/342.40 ratio is strongly density sensitive.

was identified in the 1997 spectrum (Brosius et al. 2000). The two lines in the SERTS-89 spectrum are listed in Table 10, and their intensity ratio is in agreement with the predicted value. It is to be noted that the observed intensity of the 414.68 Å line has been corrected according to the new SERTS-89 calibration proposed by Young, Landi, & Thomas (1998). The 414.68/342.39 ratio is in agreement with observations.

The SERTS 1989 flight also simultaneously recorded Ne VI lines at around 400 Å. These lines can be used, through a DEM study, to check the relative Ne-Ca abundance and test the presence of the FIP effect. The DEM of the average SERTS spectrum, as well as for two limited portions of the slit including an active region and a subflare, have been calculated by Landi (1998) by using all the strongest lines in the SERTS 1989 spectrum, the CHIANTI database (Dere et al. 1997; Young et al. 2003) and adopting the Feldman (1992) coronal abundances. This DEM has been used to calculate synthetic spectra for both Ca VII and Ne VI lines, and results are listed in Table 11, where the

TABLE 11
OBSERVED AND PREDICTED Ca VII AND Ne VI LINE INTENSITIES

| Ion | $\lambda$ (Å) | $\log T_{\mathrm{eff}}$ | $I_{\mathrm{obs}}$ | $I_{\mathrm{th}}$ |
|---|---|---|---|---|
| Ca VII .............. | 342.395 | 5.69 | $13.2 \pm 5.9$ | 13.3 |
| | 414.648[a] | 5.68 | $3.5 \pm 1.6$ | 4.3 |
| Ne VI .............. | 399.826 | 5.65 | $14.9 \pm 2.8$ | 17.1 |
| | 401.154 | 5.65 | $29.9 \pm 4.0$ | 33.1 |
| | 401.928 | 5.65 | $84.6 \pm 9.8$ | 87.1 |
| | 403.270[b] | 5.65 | $45.6 \pm 5.6$ | 19.3 |
| | 433.173[a] | 5.65 | $14.3 \pm 5.7$ | 14.7 |
| | 435.641[a] | 5.65 | $18.7 \pm 4.4$ | 24.6 |

NOTE.—Observations are from SERTS-89.

[a] Observed line intensity has been corrected following Young et al. 1998.

[b] This line is reported as blended by Thomas & Neupert 1994.

temperature of formation of the lines ($\log T_{\mathrm{eff}}$) is also displayed. The agreement between calculated and observed intensities for these two ions and the absence of systematic offsets between theoretical and experimental intensities confirm the adopted coronal abundances and demonstrate their potential for abundance diagnostics.

### 3.3. CDS Data

Two Ca VII lines have been listed by Brooks et al. (1999) in the quiet-Sun spectral atlas recorded by the Coronal Diagnostic Spectrometer (CDS; Harrison et al. 1995) on board SOHO. These two lines are close in wavelength, and their ratio can be directly calculated from the counts reported in Brooks et al. (1999). Intensities (in counts s$^{-1}$ pixel$^{-1}$) and line ratios are listed in Table 10. The calculated intensity ratio is in agreement with observations, although its experimental uncertainty is rather high.

Ca VII lines are routinely observed in CDS spectra. As an example, we have analyzed the Ca VII lines observed in an active region spectrum observed with the Normal Incidence Spectrometer (NIS) of CDS. The NIS is composed of two channels observing in the 308–381 Å (NIS 1) and 513–633 Å (NIS 2) wavelength ranges simultaneously. The spectrum was observed on 1998 April 14 and consists of a full CDS spectrum of a limited ($20'' \times 240''$) portion of an active region recorded as part of the standard full NIS spectrum program (NISAT program). The observation was centered at ($31''$, $306''$) in heliocentric coordinates, and consisted of 10 consecutive exposures, each 51 s long and shifted relative to the previous by $2''$ along the solar east-west direction. A small portion of the field of view, where transition region lines were strongest, was selected for the analysis. Both the field of view and the selected region are displayed in Figure 3; images are taken at several different temperatures, corresponding to emission lines in the solar chromosphere, transition region, and corona. A few Ca VII lines have been identified, and their intensities and line ratios are reported in Table 10. It is possible to see that the 342.45 and 339.92 Å
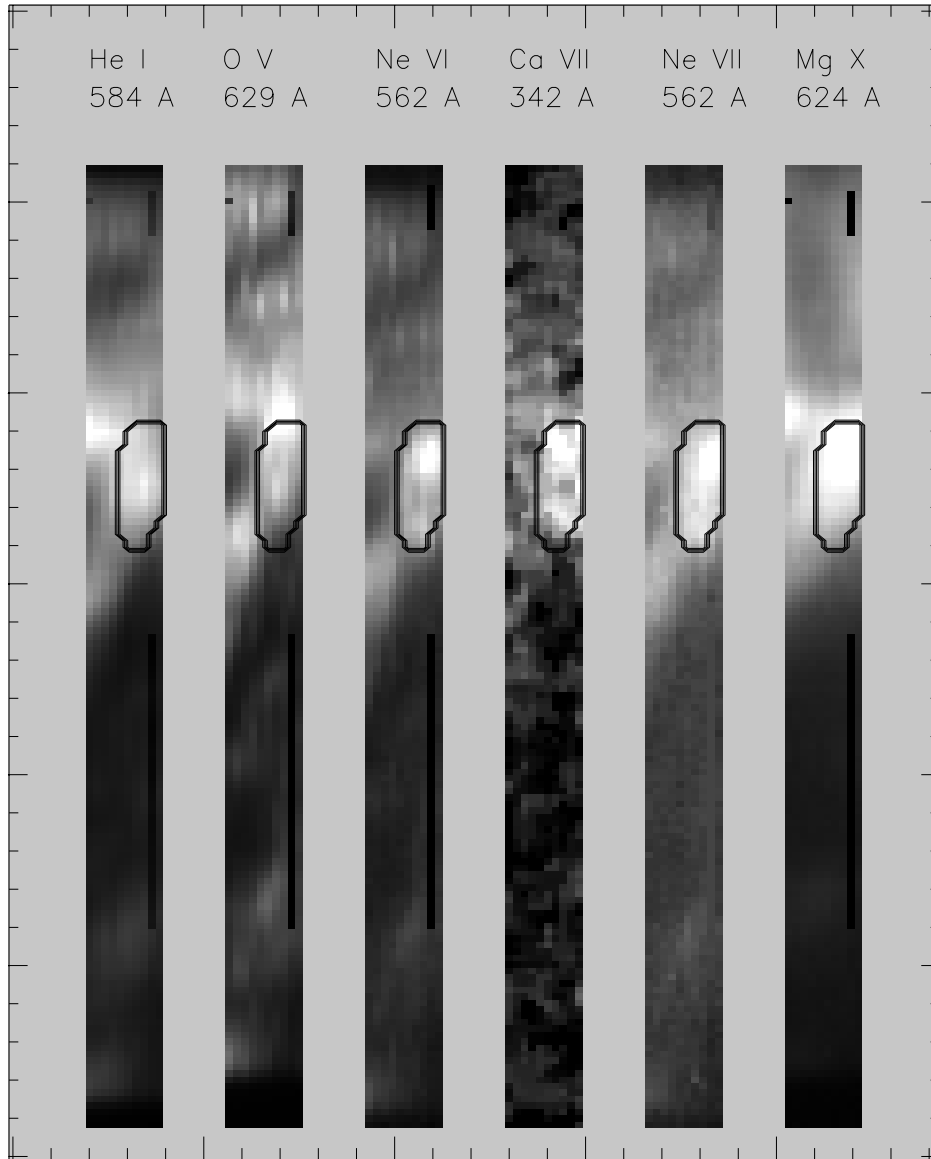
Fig. 3.—Active region monochromatic images observed by CDS. The field of view of each panel is centered at $(31'', 306'')$. Each image corresponds to a narrow temperature range: He I, $3 \times 10^4$ K; O V, $2 \times 10^5$ K; Ne VI, $5 \times 10^5$ K; Ca VII, $5 \times 10^5$ K; Ne VII, $6 \times 10^5$ K; Mg X, $1 \times 10^6$ K (Mazzotta et al. 1998). The contours mark the region used for the present analysis.

lines are in agreement with observations. The 340.72 Å is probably blended with a stronger unidentified transition, as its observed intensity exceeds the predicted one by a factor of 4. The 330.01 Å line is also blended, as its observed intensity is a factor of 1.9–75 higher than the maximum value predicted by the theoretical calculation. This line cannot be used for density diagnostics in the present spectrum. The line identified at 551.47 Å provides temperature-sensitive line ratios with lines at around 350 Å. Table 10 shows that the 551.47/342.39 line ratio provides a temperature of $\log T \leq 5.55$ ($T$ in K), close to the Ca VII temperature of maximum abundance. However, it is possible that some blending contribution from a Si X doublet, predicted by CHIANTI at 551.2 Å and not resolved by CDS, contaminates the Ca VII 551.47 line, so that the measured temperature is underestimated.

The active region spectrum also includes some Ne VI lines in the NIS 2 wavelength channel, so that relative abundance studies are possible with these two ions. In order to determine the relative abundance of these two elements, the DEM of the emitting plasma was determined using the lines observed in both the NIS 1 and NIS 2 section of CDS, using the iterative procedure developed by Landi & Landini (1997). The abundances adopted to determine the DEM were from Feldman (1992). The derived DEM has been used to compute synthetic spectra for both Ne VI and Ca VII, and the results are reported in Table 12. It can be seen that there are no systematic differences between predicted and observed line intensities, so that the adopted Feldman (1992) coronal abundances are confirmed.

## 4. CONCLUSIONS

In the present work we have carried out ab initio calculations of energy levels, transition rates, and collisional

TABLE 12
Observed and Predicted Ca VII and Ne VI Line Intensities

| Ion | $\lambda$ (Å) | $\log T_{\rm eff}$ | $I_{\rm obs}$ (ergs cm$^{-2}$ s$^{-1}$ sr$^{-1}$) | $I_{\rm th}$ (ergs cm$^{-2}$ s$^{-1}$ sr$^{-1}$) |
|---|---|---|---|---|
| Ca VII .............. | 339.967 | 5.72 | $11.8 \pm 2.7$ | 10.6 |
|  | 340.701 | 5.72 | $16.9 \pm 2.6$ | 5.0 |
|  | 342.395 | 5.72 | $19.0 \pm 2.2$ | 22.6 |
| Ne VI .............. | 558.592 | 5.68 | $41.3 \pm 4.0$ | 45.8 |
|  | 562.798 | 5.68 | $73.6 \pm 7.5$ | 88.8 |

Note.—Measured line intensities are from an active region observed from CDS.

excitation rates for the Si-like ion Ca VII. Calculations were performed using the University College London suite of codes, which adopts the distorted-wave (DW) approximation to solve the electron-ion scattering problem. The calculations were carried out at seven values of the incident electron energy (8, 10, 15, 20, 30, 40, and 60 ryd) and by including intermediate angular momentum states $L^T$ up to 32. Transition rates were calculated for all possible transitions in the atomic model. The transition rates resulting from the present work are compared with earlier computations, where available, and satisfactory agreement is found. Their reliability is discussed in light of atomic model completeness.

The theoretical data have been used to calculate level populations and line emissivities, to be compared with observations. Line intensity ratios calculated from the present data set compare favorably with the values observed by the SERTS and CDS instruments on quiet-Sun and active regions. Ca VII line ratios can be used for plasma diagnostics in the solar transition region.

We demonstrate that Ca VII and Ne VI lines are formed at similar temperatures, thus providing a very useful tool to determine the Ca/Ne relative abundance. Given their first ionization potential (FIP), Ca and Ne can be used to investigate the FIP effect in the solar plasmas. As an example, using SERTS and CDS observations, we check that the relative Ne/Ca abundance is consistent with the Feldman (1992) coronal set of abundances, thus confirming that the plasma is affected by the FIP effect.

The present data set represents the first effort to provide a self-consistent, complete set of data to calculate Ca VII level populations and line emissivities. These data are available to users in electronic files and will be included in the next release of the CHIANTI database.

REFERENCES

Allen, C. W. 1973, Astrophysical Quantities (London: Athlone Press)
Brooks, D. H., et al. 1999, A&A, 347, 277
Brosius, J. W., Thomas, R. J., Davila, J. M., & Landi, E. 2000, ApJ, 543, 1016
Burgess, A., & Shoerey, V. B. 1974, J. Phys. B, 7, 2403
Burgess, A., & Tully, J. A. 1992, A&A, 254, 436
Del Zanna, G., Landini, M., & Mason, H. E. 2002, A&A, 385, 968
Dere, K. P., Landi, E., Mason, H. E., Monsignori Fossi, B. C., & Young, P. R. 1997, A&AS, 125, 149
Desclaux, J. P. 1975, Comput. Phys. Commun., 9, 31
Eissner, W. 1998, Comput. Phys. Commun., 114, 295
Eissner, W., Jones, M., & Nussbaumer, H. 1974, Comput. Phys. Commun., 8, 270
Eissner, W., & Seaton, M. J. 1972, J. Phys. B, 5, 2187
Ekberg, J. O., & Svensson, L. A. 1970, Phys. Scr., 2, 283
Ekefors, E. 1931, Zeits. Phys., 71, 53
Fawcett, B. C. 1987, At. Data Nucl. Data Tables, 36, 129
Feldman, U. 1992, Phys. Scr., 46, 202
Fuhr, J. R., et al. 1999, NIST Atomic Spectra Database Version 2.0 (NIST Physical Reference Data)
Galavis, M. E., Mendoza, C., & Zeippen, C. J. 1995, A&AS, 111, 347
Harrison, R. A., et al. 1995, Sol. Phys., 162, 233

Huang, K.-N. 1985, At. Data Nucl. Data Tables, 32, 503
Kelly, R. L. 1987, J. Phys. Chem. Ref. Data, 16, Suppl. 1
Krueger, T. K., & Czyzak, S. J. 1966, ApJ, 144, 1194
Landi, E. 1998, Ph.D. thesis, Univ. Florence
Landi, E., & Landini, M. 1997, A&A, 327, 1230
Malville, J., & Berger, R. A. 1965, Planet. Space Sci., 13, 1131
Mazzotta, P., Mazzitelli, G., Colafrancesco, S., & Vittorio, N. 1998, A&AS, 133, 403
Phillips, L. W. 1939, Phys. Rev., 55, 708
Saraph, H. E. 1978, Comput. Phys. Commun., 15, 24
Saraph, H. E., & Eissner, W. 2003, Comput. Phys. Commun., submitted
Smitt, R., Svensson, L. A., & Outred, M. 1976, Phys. Scr., 13, 293
Swings, P., & Struve, O. 1940, ApJ, 91, 546
———. 1941, ApJ, 94, 291
Thackeray, A. D. 1974, MNRAS, 167, 87
Thomas, R. J., & Neupert, W. M. 1994, ApJS, 91, 461
Varsavsky, C. M. 1961, ApJS, 6, 75
Whitford, A. E. 1934, Phys. Rev., 46, 793
Young, P. R., Del Zanna, G., Landi, E., Dere, K. P., Mason, H. E., & Landini, M. 2003, ApJS, 144, 135
Young, P. R., Landi, E., & Thomas, R. J. 1998, A&A, 329, 291
Young, P. R., & Mason, H. E. 1997, Sol. Phys., 175, 523